Bioorganic Chemistry 92 (2019) 103285

Contents lists available at ScienceDirect

Bioorganic Chemistry

journal homepage: www.elsevier.com/locate/bioorg

2-Styrylchromone derivatives as potent and selective monoamine oxidase B inhibitors

Koichi Takao[a,*], Saki Endo[a], Junko Nagai[b], Hitoshi Kamauchi[a], Yuri Takemura[a], Yoshihiro Uesawa[b], Yoshiaki Sugita[a]

[a] Laboratory of Bioorganic Chemistry, Department of Pharmaceutical Sciences, Faculty of Pharmacy and Pharmaceutical Sciences, Josai University, 1-1 Keyaki-dai, Sakado, Saitama 350-0295, Japan
[b] Department of Medical Molecular Informatics, Meiji Pharmaceutical University, 2-522-1 Noshio, Kiyose, Tokyo 204-8588, Japan

ARTICLE INFO

Keywords:
2-Styrylchromone
Monoamine oxidase-A
Monoamine oxidase-B
Quantitative structure–activity relationship
Molecular Operating Environment
AutoGPA

ABSTRACT

A series of eighteen 2-styrylchromone derivatives (see Chart 1) were synthesized and evaluated for their monoamine oxidase (MAO) A and B inhibitory activities. Many of the derivatives inhibited MAO-B comparable to pargyline (a positive control), and most of them inhibited MAO-B selectively. Of the eighteen derivatives, compound **9** having methoxy group at R^1 and chlorine at R^4 showed both the best MAO-B inhibitory activity (IC_{50} = 17 ± 2.4 nM) and the best MAO-B selectivity (IC_{50} for MAO-A/IC_{50} for MAO-B = 1500). The mode of inhibition of compound **9** against MAO-B was competitive and reversible. Quantitative structure–activity relationship (QSAR) analyses of the 2-styrylchromone derivatives were conducted using their pIC_{50} values with the use of Molecular Operating Environment (MOE) and Dragon, demonstrating that the descriptors of MAO-B inhibitory activity and MAO-B selectivity were 1734 and 121, respectively, that showed significant correlations ($P < 0.05$). We then examined the 2-styrylchromone structures as useful scaffolds through three-dimensional-QSAR studies using AutoGPA, which is based on the molecular field analysis algorithm using MOE. The model using pIC_{50} value indexes for MAO-B exhibited a determination coefficient (R^2) of 0.873 as well as a Leave-One-Out cross-validated determination coefficient (Q^2) of 0.675. These data suggested that the 2-styrylchromone structure might be a useful scaffold for the design and development of novel MAO-B inhibitors.

1. Introduction

Monoamine oxidase (MAO, EC 1.4.3.4) is a flavoenzyme bound to the mitochondrial outer membranes of many types of mammalian cells. MAO catalyzes the oxidative deamination of endogeneous and exogeneous amines, including neurotransmitters such as epinephrine, dopamine, and serotonin [1]. Human has two types of MAO, MAO-A and MAO-B, which share approximately 70% sequence identity at the amino acid level and are identified based on their substrate and inhibitor sensitivities [2,3]. MAO-A preferentially deaminates epinephrine, norepinephrine and serotonin, and is inhibited irreversibly by clorgyline. MAO-B preferentially deaminates benzylamine, β-phenethylamine and dopamine, and is inhibited irreversibly by (*R*)-(-)-deprenyl, a drug for the treatment of Parkinson's disease. As the concentration change of the neurotransmitters in the brain linked to various neurodegenerative diseases' pathologies, many laboratories have engaged in the development of inhibitors of the two enzymes [4].

Derivatives of chromone (4*H*-1-benzopyran-4-one) are widely distributed in plants and are scaffolds for MAO inhibitors [5–7]. Flavone (2-phenylchromone) and isoflavone (3-phenylchromone) including their derivatives constitute a large group of naturally occurring chromones, while 2-styrylchromone and its derivatives a small group [8,9]. Synthetic 2-styrylchromones were evaluated for a number of biological activities, such as antioxidant, anti-inflammatory, anti-allergic, antitumor, and antiviral activities [8,9], but their inhibitory activity against MAO has not been reported. On the other hand, a natural product resveratrol (3,5,4′-trihydroxy-*trans*-stylbene) has been well studied because of its numerous biological effects [10,11]. Regarding the inhibition of MAO, *cis*-resveratrol is less effective than *trans*-resveratrol [12]. Hence, the related *trans*-stilbene-type compounds such as (*E*)-2-styryl-2-imidazoline [13], (*E*)-styrylcaffeine [14,15], (*E*)-2-styrylbenzimidazole [15], (*E*)-styrylisatin [16], (*E*)-styrylxanthine derivatives [17], and 3-(*E*)-styryl-2*H*-chromene derivatives [18] were reported as MAO inhibitors. These findings suggested that 2-styrylchromones had a potential to inhibit MAO.

In order to further explore new biological activities of this family of

* Corresponding author.
E-mail address: ktakao@josaiac.jp (K. Takao).

https://doi.org/10.1016/j.bioorg.2019.103285
Received 11 July 2019; Received in revised form 28 August 2019; Accepted 15 September 2019
Available online 18 September 2019
0045-2068/

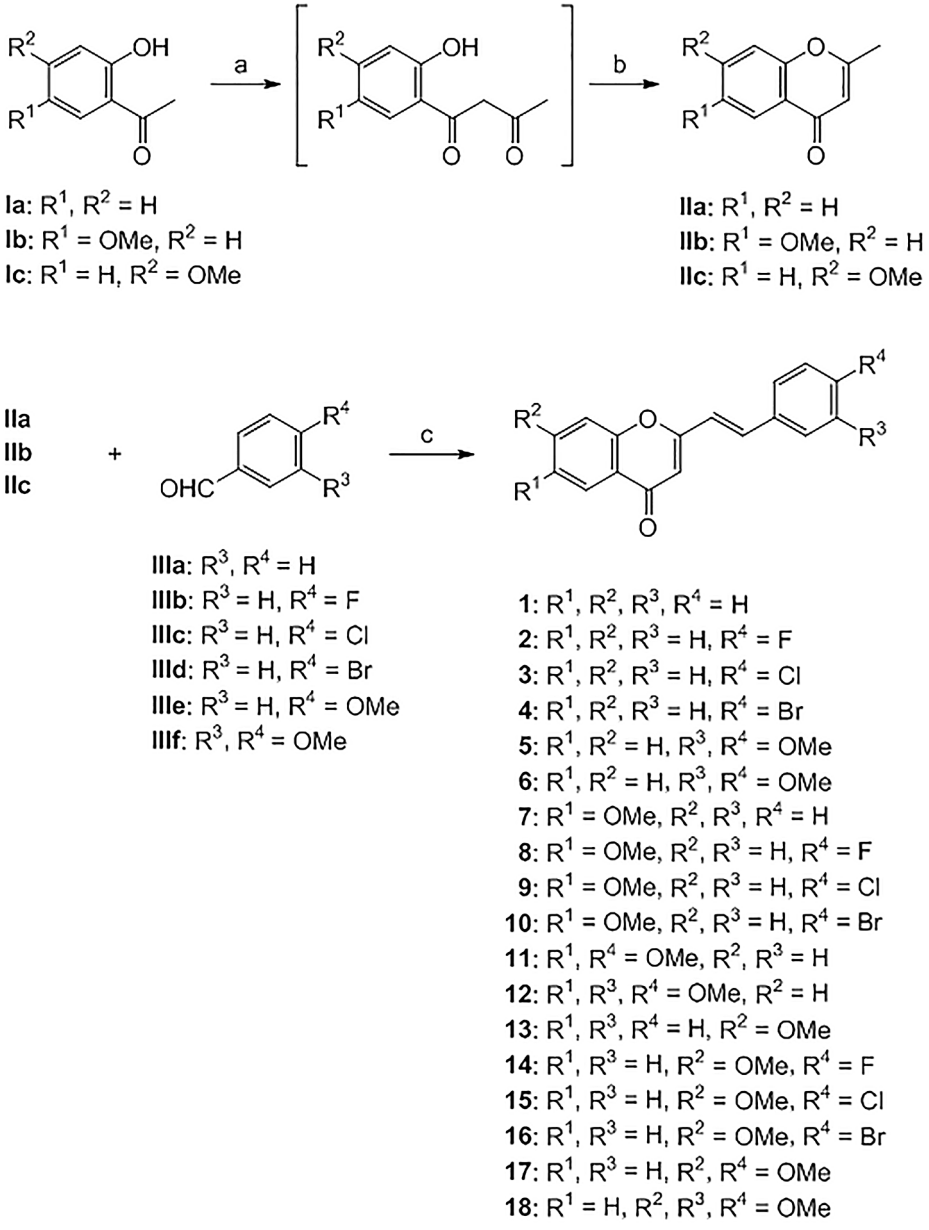

Chart 1. Synthetic protocol for 2-styrylchromone derivatives. Reagents and conditions: (a) Na, AcOEt, rt; (b) conc. HCl, MeOH, rt; (c) NaOMe, MeOH, reflux.

compounds, we synthesized a series of 2-styrylchromone derivatives (Chart 1). This paper also deals with their inhibitory activities against human MAO-A and MAO-B, and from the results studies on the quantitative structure–activity relationship (QSAR) analyses of the derivatives to MAO-B.

2. Results and discussion

2.1. Chemistry

2.1.1. Synthesis of 2-styrylchromone derivatives

2-Styrylchromone derivatives (**1**–**18**) were synthesized as shown in Chart 1. 2-Methylchromone derivatives (**IIa-c**) were first synthesized by Claisen condensation of the corresponding acetophenone derivatives (**Ia-c**) with ethyl acetate, followed by intramolecular cyclization as described previously [19]. Then the resulting **IIa-c** reacted with each benzaldehyde derivative (**IIIa-f**) in the presence of base using a modification of the previous procedure [19] to obtain corresponding 2-styrylchromone derivatives.

2.2. Biological activity

2.2.1. Inhibitory activity towards MAO-A and MAO-B

All the eighteen 2-styrylchromone derivatives were evaluated for MAO-A and MAO-B inhibitory activities. As shown in Table 1, modifications of chromone ring (R^1,R^2) and of phenyl ring (R^3,R^4) on 2-styrylchromone revealed several interesting structure-activity relationships.

The MAO-A inhibitory activities of the derivatives were determined. Compounds **1**, **2**, **3**, **4**, **5**, **7**, **8**, **10** and **11**, more or less, showed inhibitory activities, and Compound **8** inhibited MAO-A most potently (IC_{50} = 0.12 ± 0.0060 μM). Substitution of methoxy group at R^1 seemed to intensify MAO-A inhibitory activities, such as compound **1** vs. **7**, **2** vs. **8**, **4** vs. **10** and **5** vs. **11**, but with an exception of compound **3** vs. **9**. And substitution of methoxy group at R^2 weakened MAO-A inhibitory activities without exception such as compound **1** vs. **13**, **2** vs. **14**, **3** vs. **15**, **4** vs. **16**, **5** vs. **17** and **6** vs. **18**.

The MAO-B inhibitory activities of the derivatives were then determined, and all the derivatives were found to inhibit MAO-B more

Table 1
The IC_{50} values and selectivity of 2-styrylchromone derivatives for the inhibition of MAO-A and MAO-B. MAO-B selectivity is given as the ratio of the IC_{50} value for MAO-A/IC_{50} value for MAO-B. All values are expressed as the mean ± standard deviation of triplicate determinations.

Compd.	R1	R2	R3	R4	MAO-A IC50 (μM)	MAO-B IC50 (μM)	MAO-B selectivity
1	H	H	H	H	0.95 ± 0.030	0.24 ± 0.024	4
2	H	H	H	F	0.59 ± 0.032	0.17 ± 0.013	4
3	H	H	H	Cl	0.29 ± 0.025	0.079 ± 0.0013	4
4	H	H	H	Br	0.33 ± 0.0050	0.069 ± 0.0045	5
5	H	H	H	OMe	2.3 ± 0.073	0.049 ± 0.0013	47
6	H	H	OMe	OMe	25 ± 0.81	2.8 ± 0.32	9
7	OMe	H	H	H	0.20 ± 0.012	0.18 ± 0.0027	1
8	OMe	H	H	F	0.12 ± 0.0060	0.064 ± 0.0025	2
9	OMe	H	H	Cl	26 ± 3.5	0.017 ± 0.0024	1500
10	OMe	H	H	Br	0.53 ± 0.010	0.024 ± 0.0024	22
11	OMe	H	H	OMe	0.21 ± 0.047	0.19 ± 0.014	1
12	OMe	H	OMe	OMe	21 ± 0.47	0.68 ± 0.022	31
13	H	OMe	H	H	26 ± 1.1	0.22 ± 0.0095	120
14	H	OMe	H	F	35 ± 4.4	0.12 ± 0.010	290
15	H	OMe	H	Cl	> 100	0.27 ± 0.021	> 370
16	H	OMe	H	Br	> 100	0.45 ± 0.010	> 220
17	H	OMe	H	OMe	72 ± 1.3	1.4 ± 0.039	51
18	H	OMe	OMe	OMe	> 100	10 ± 1.1	> 10
Pargyline					4.6 ± 0.27	0.22 ± 0.024	21

potently than MAO-A. Compound **9** was the most potent inhibitor (IC_{50} = 17 ± 2.4 nM), showing the inhibitory activity of approximately 13-fold as much as that of pargyline (a positive control). Compounds **3**, **4**, **5**, **8**, and **10** showed more potent inhibition than pargyline, and compounds **1**, **2**, **7**, **11**, **12**, **13**, **14**, **15** and **16** showed a similar inhibition to pargyline. Substitution of methoxy group at R^1 seemed to intensify MAO-B inhibitory activities, such as compound **2** vs. **8**, **3** vs. **9**, **4** vs. **10** and **6** vs. **12**, but with an exception of compound **5** vs. **11**. And substitution of methoxy group at R^2 seemed to weaken MAO-B inhibitory activities, such as compound **3** vs. **15**, **4** vs. **16**, **5** vs. **17** and **6** vs. **18**, but with similar value of compound **1** vs. **13** or **2** vs. **14**.

MAO-B selectivities of the derivatives were then calculated, defined as the ratio of IC_{50} value of MAO-A to that of MAO-B for each derivative. Of the derivatives compound **9** showed a significantly high MAO-B selectivity (1500). Thus, compound **9**, the most potent MAO-B inhibitor, was chosen for the following kinetics study (Fig. 1). From the Lineweaver–Burk plots, the mode of MAO-B inhibition was competitive and reversible with Ki value of 8 nM, suggesting a tight fitting of

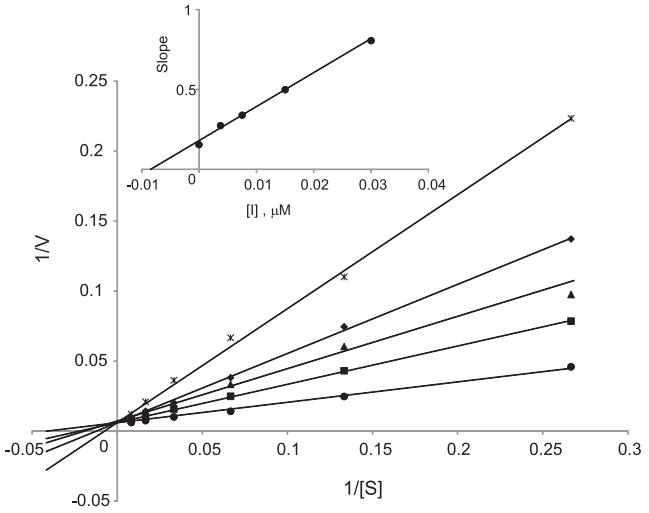

Fig. 1. Lineweaver–Burk plots for the inhibition of MAO-B by compound **9**. The plots were constructed in the absence (filled circles) and presence (other symbols) of various concentrations of compound **9**. The inset is a graph of the slopes of the Lineweaver–Burk plots versus inhibitor concentration (Ki = 0.0080 μM). The rate (V) is expressed as % of control. Kynuramine was used at 30 μM.

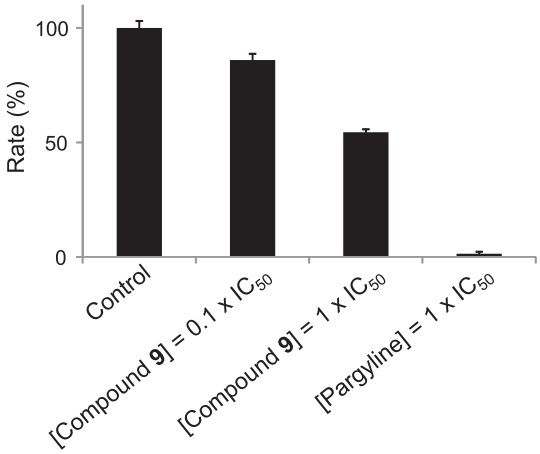

Fig. 2. The reversibility of inhibition of MAO-B by compound **9**. MAO-B was preincubated with compound **9** at 10 × IC_{50} and 100 × IC_{50} for 30 min and then diluted to 0.1 × IC_{50} and 1 × IC_{50}, respectively. For comparison, the irreversible MAO-B inhibitor pargyline at 10 × IC_{50} was similarly incubated with MAO-B and diluted to 1 × IC_{50}. The residual activity of MAO-B was subsequently measured.

compound **9** to MAO-B active site. The reversibility of MAO-B inhibition by compound **9** was further confirmed in contrast to the irreversibility of pargyline according to the literature method [20] (Fig. 2).

2.2.2. Computational analyses

2-Styrylchromone derivatives showed potent MAO-B inhibitory activity and selectivity. The statistical significance ($P < 0.05$) of each substituted group was computationally analyzed (Fig. 3) and showed that the substitution of methoxy group at R^2 significantly affected both MAO-B inhibitory activity ($P = 0.0440$) and selectivity ($P = 0.0130$). Other substitutions at R^1, R^2, R^3 and R^4 had no significant effect on either MAO-B inhibitory activity or selectivity. These data suggested that the 2-styrylchromone scaffold is a useful candidate structure for the design of MAO-B selective inhibitors.

In an effort to elucidate further the structure activity relationships between MAO-B and inhibitors, quantitative structure–activity relationship (QSAR) analyses of 2-styrylchromone derivatives were conducted using Molecular Operating Environment (MOE) [21] and Dragon [22] (a total of 3106 descriptors).

QSAR analyses were performed for 2-styrylchromone derivatives

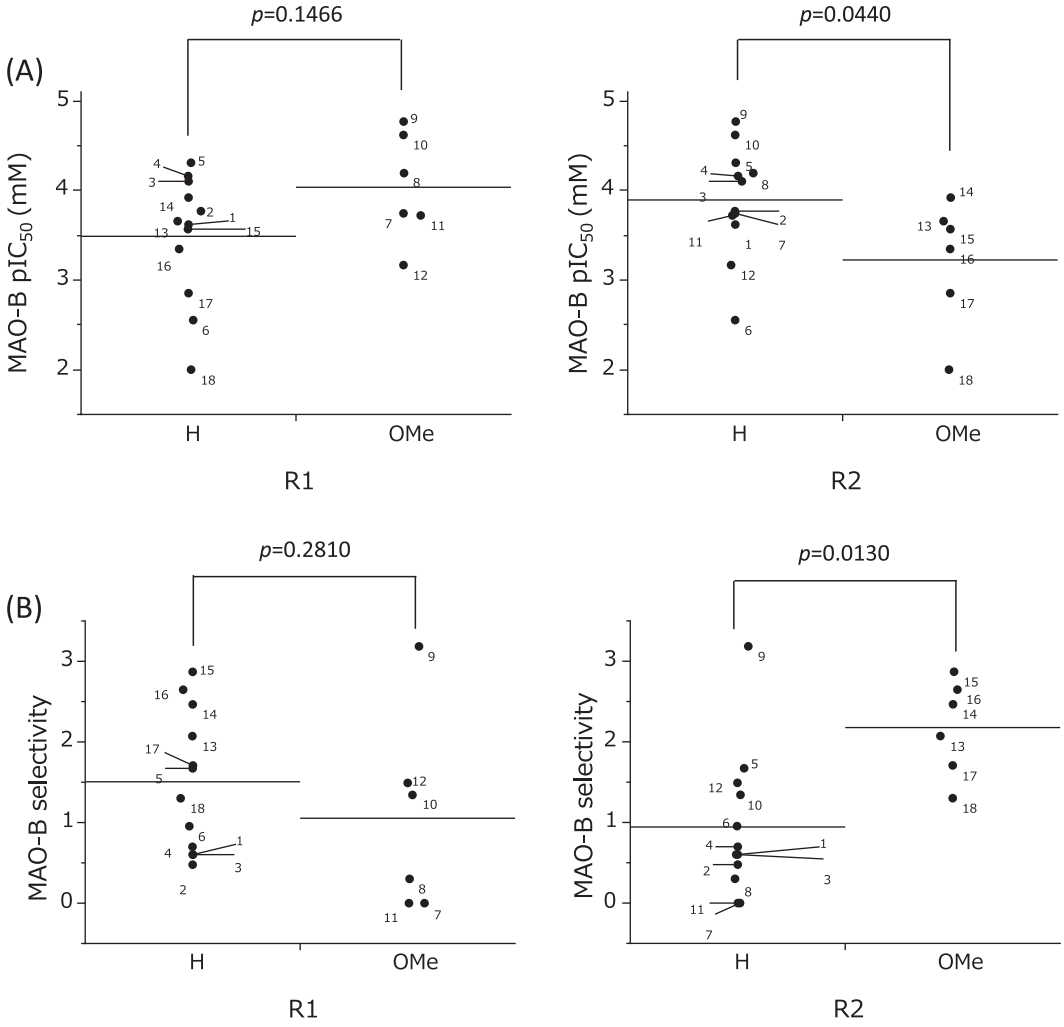

Fig. 3. Effect of substitutions at R^1 and R^2 of 2-styrylchromone derivatives on MAO-B inhibition and selectivity.

with pIC_{50} values for MAO-B inhibitory activity and exhibiting MAO-B selectivity. These analyses demonstrated that 1734 and 121 descriptors showed significant correlations ($P < 0.05$) for MAO-B inhibitory activity and selectivity, respectively. Scatter plots of the top six descriptors are shown in Figs. 4, 5. The strongly correlated descriptors indicated that properties such as molecular size, shape, and the electronic state of 2-styrylchromone derivatives are important for their inhibitory activity and selectivity. These structural and physicochemical properties suggested that the binding of 2-styrylchromone derivatives to the binding site of MAO-B is stabilized by van der Waals forces and electrostatic interactions. We also performed three-dimensional-QSAR (3D-QSAR) studies on the eighteen compounds exhibiting MAO-B inhibitory activity using AutoGPA based on the molecular field analysis (CoMFA) algorithm [23] using MOE [24]. Developed models supporting the prediction of pIC_{50} and pSelectivity for MAO-B provided values that correlated with the corresponding experimental values, as shown in Fig. 6. The pIC_{50} and pSelectivity values had determination coefficients (R^2) of 0.873 and 0.867, respectively, and Leave-One-Out cross-validated determination coefficients (Q^2) of 0.675 and 0.483, respectively. In this analysis, $Q^2 > 0.5$ suggested that the model is reasonable and should have good predictive ability [25], and that the model for MAO-B inhibition provides reasonable pIC_{50} values. The contour map of the AutoGPA-based model of MAO-B pIC_{50} values is shown in Fig. 7A. In the electrostatic contour map, the blue contour suggests electropositive charge and the red contour suggests electronegative charge that likely help increase activity, whereas in the steric contour map, the green contour represents bulky groups favorable for increasing activity and the yellow contour indicates decreased activity.

A molecular docking study performed using the MOE-Dock function was conducted to better understand the developed model (Fig. 7b, c). The interactions between compound **9** with MAO-B protein (PDB code 4A79) were investigated using MOE. The interaction with the pharmacophore moieties F1 and F2 in Fig. 7A corresponds to the interaction with Ile171 and Ile199 in Fig. 7B and C, respectively. The green contour in Fig. 7A located over the chromone ring likely corresponds to FAD in Fig. 7B, supporting our observation that substitution with a methoxy group at R^1 increases MAO-B inhibitory activity. The 3D-QSAR model correlated well with the molecular docking results.

A recent review [26] reported that the active site structure of human MAO-B has a bipartite hydrophobic cavity comprising an entrance cavity and a substrate cavity. The structure of the cavity is mainly determined by an entrance loop (residues 99–110) that regulates ligand access to the active site, and a cavity-shaping loop formed by residues 200–209. The substrate cavity in MAO-B has a volume of ~430A^3 and the entrance cavity has a volume of ~290 Å^3. The combined volume of the two cavities when the gating Ile199 is in its open conformation is ~700 Å^3. Tyr326 is another important residue for gating. Interestingly, compound **9** interacted with both Ile199 and Tyr326, as shown in Fig. 7C. Furthermore, the above-mentioned review reported that Tyr398 and Tyr435 stack parallel to each other and perpendicular to the FAD ring, creating an aromatic sandwich that stabilizes substrate binding. We also observed their interactions Tyr398 and Tyr435, as shown in Fig. 7C. The active site of MAO-A has a

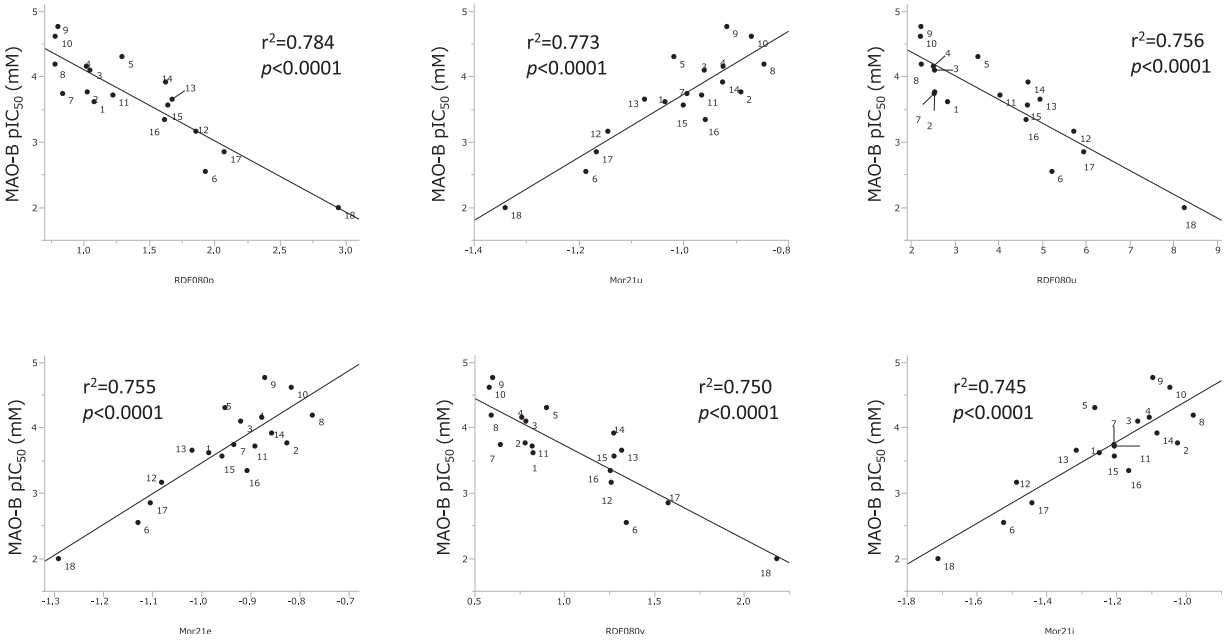

RDF080p	dragon	3D shape and polarizability	Radial Distribution Function - 080 / weighted by polarizability
Mor21u	dragon	3D shape	signal 21 / unweighted
RDF080u	dragon	3D shape	Radial Distribution Function - 080 / unweighted
Mor21e	dragon	3D shape and electric state	signal 21 / weighted by Sanderson electronegativity
RDF080v	dragon	3D shape and size	Radial Distribution Function - 080 / weighted by van der Waals volume
Mor21i	dragon	3D shape and ionization potential	signal 21 / weighted by ionization potential

Fig. 4. Determination of the coefficient between the chemical descriptors and the pIC_{50} values of 2-styrylchromone derivatives for MAO-B.

monopartite cavity with a total volume of ~550 Å^3. It therefore appears that MAO-B recognizes its substrate less stringently than MAO-A. Therefore, 2-styrylchromene derivatives might be selective for MAO-B.

Recently, our group reported the MAO-B inhibitory activities of 3-(*E*)-styryl-2*H*-chromene derivatives [18]. Resveratrol inhibits MAO-A more strongly than MAO-B. In contrast, the related compounds (*E*)-2-styryl-2-imidazoline [13], (*E*)-styrylcaffeine [14] and (*E*)-styrylisatin derivatives [16] showed more potent MAO-B inhibition than MAO-A inhibition. These results suggest that the styryl moiety of these derivatives prefers to bind to the substrate cavity of MAO-B compared to the MAO-A cavity. Docking study on MAO-B has been done using (*E*)-styrylisatin derivatives [16], and the isatin moiety of both C-5 and C-6 styrylisatin was located in the substrate cavity and the styryl moiety extended to the entrance cavity of MAO-B. This was similar to the direction of 2-styrylchromone derivatives in MAO-B active site.

This is the first report identifying 2-styrylchromone derivatives as potent MAO-B inhibitors. The results suggest that the 2-styrylchromone structure may be a useful scaffold for the design and development of novel MAO-B inhibitors.

3. In conclusion

The present study demonstrated that 2-styrylchromone derivatives were potent and selective MAO-B inhibitors. Of eighteen derivatives synthesized, fifteen showed potent MAO-B inhibitory activities, and sixteen showed MAO-B selectivity. Especially, compound **9,** having a methoxy group at R^1 and chlorine at R^3, exhibited the highest MAO-B inhibitory activity and selectivity. Computational analyses also suggested the influence of substitution by methoxy group at R^1. QSAR and 3D-QSAR analyses suggested that 2-styrylchromone derivatives would be a promising scaffold for the design and development of new MAO-B inhibitors.

4. Experimental

4.1. Chemistry

All reagents and solvents were purchased from commercial sources. Analytical thin-layer chromatography was performed on silica-coated plates (silica gel 60F-254; Merck Ltd., Tokyo, Japan) and visualized under UV light. Column chromatography was carried out using silica gel (Wakogel C-200; Wako Pure Chemical Industry Co., Tokyo, Japan). All melting points were determined using a Yanagimoto micro-hot stage and are uncorrected. ^{1}H NMR and ^{13}C NMR spectra were recorded on a Varian 400-MR spectrometer using tetramethylsilane as an internal standard. MS spectra were measured using a JEOL JMS-700 spectrometer. Elemental analyses were carried out on a Yanaco CHN MT-6 elemental analyzer.

4.1.1. Synthesis of 2-methylchromones

2-Methylchromones (**IIa-c**) were synthesized according to previous methods [19]. To a solution of the corresponding acetophenone (**I**, 20 mmol) in dry ethyl acetate (30 mL), sodium (120 mmol) was added. The reaction mixture was stirred for 18 h at room temperature. After

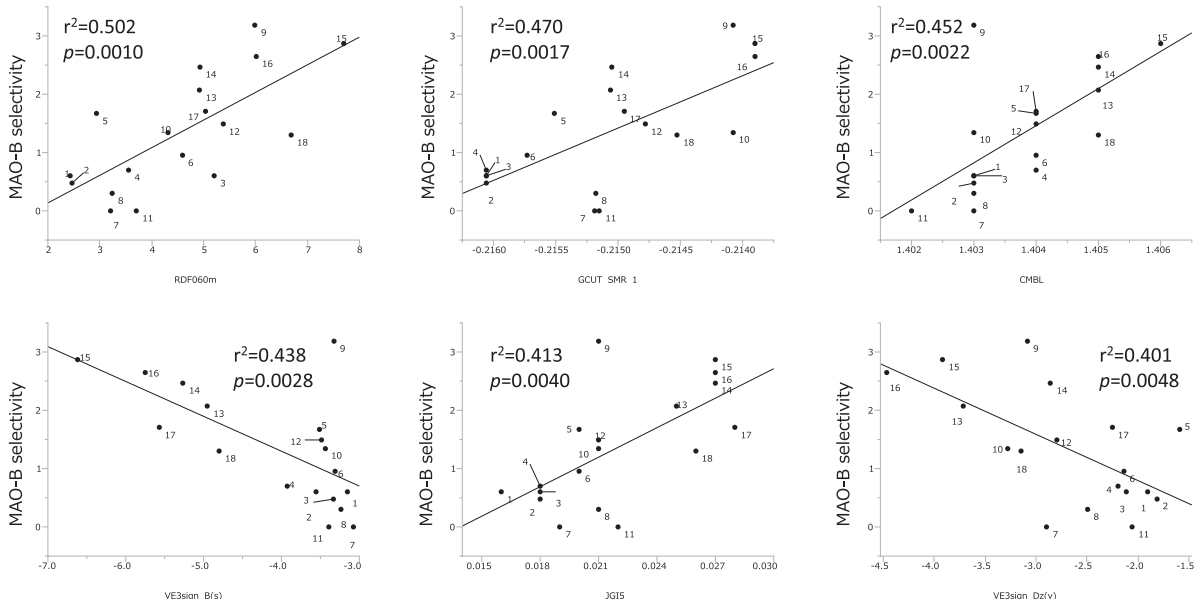

RDF060m	dragon	3D shape and size	Radial Distribution Function - 060 / weighted by mass
GCUT_SMR_1	MOE	topological shape	The GCUT descriptors using atomic contribution to molar refractivity (using the Wildman and Crippen SMR method) instead of partial charge.
CMBL	dragon	3D shape and size	conjugated maximum bond length
VE3sign_B(s)	dragon	topological shape and electric state	logarithmic coefficient sum of the last eigenvector from Burden matrix weighted by I-State
JGI5	dragon	topological shape and electric state	mean topological charge index of order 5
VE3sign_Dz(v)	dragon	topological shape and size	logarithmic coefficient sum of the last eigenvector from Barysz matrix weighted by van der Waals volume

Fig. 5. Determination of the coefficient between the chemical descriptors and the MAO-B selectivity of 2-styrylchromone derivatives.

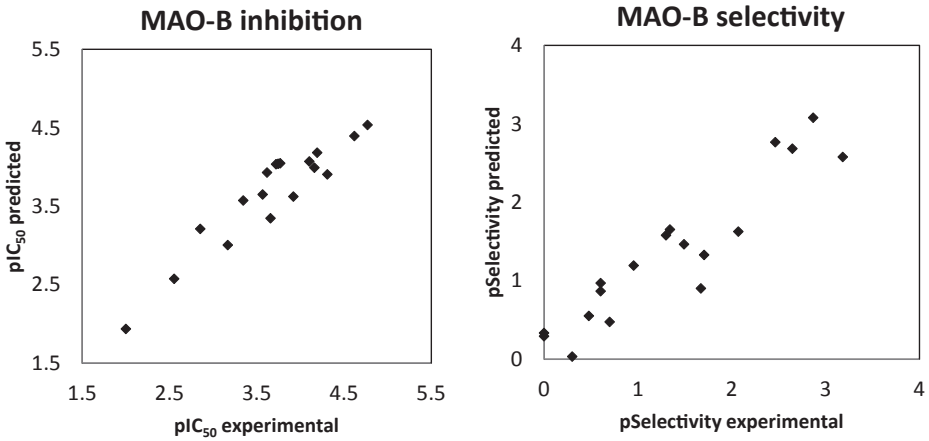

Fig. 6. Graphs of the predicted and experimental pIC_{50} MAO-B inhibition and pSelectivity MAO-B selectivity values for 2-styrylchromone derivatives.

the reaction mixture was diluted with ice-water and acidified with 2 M HCl, the aqueous layer was separated and extracted with ethyl acetate. The combined organic layer was dried over Na_2SO_4 and the solvent was evaporated under reduced pressure to obtain the crude diketone. A solution of the crude diketone with a few drops of conc. HCl in MeOH (50 mL) was stirred for 4 h at room temperature. MeOH was removed under reduced pressure, ethyl acetate was added, and the solution was washed with brine. The organic layer was dried over Na_2SO_4 and the solvent was evaporated under reduced pressure. The residue was purified by silica gel column chromatography (hexane:AcOEt = 10:1) to give the title compounds. The products (**IIa-c**) were identified by their melting points and ^{1}H NMR spectra [19,27].

4.1.2. 2-Methyl-4H-1-benzopyran-4-one (IIa)

Yield 51%. Pale brown scaly crystal. mp 71–73 °C (lit. [27] 70–72 °C). ^{1}H NMR ($CDCl_3$, 400 MHz) δ 8.19 (1H, dd, J = 7.9, 1.7 Hz,

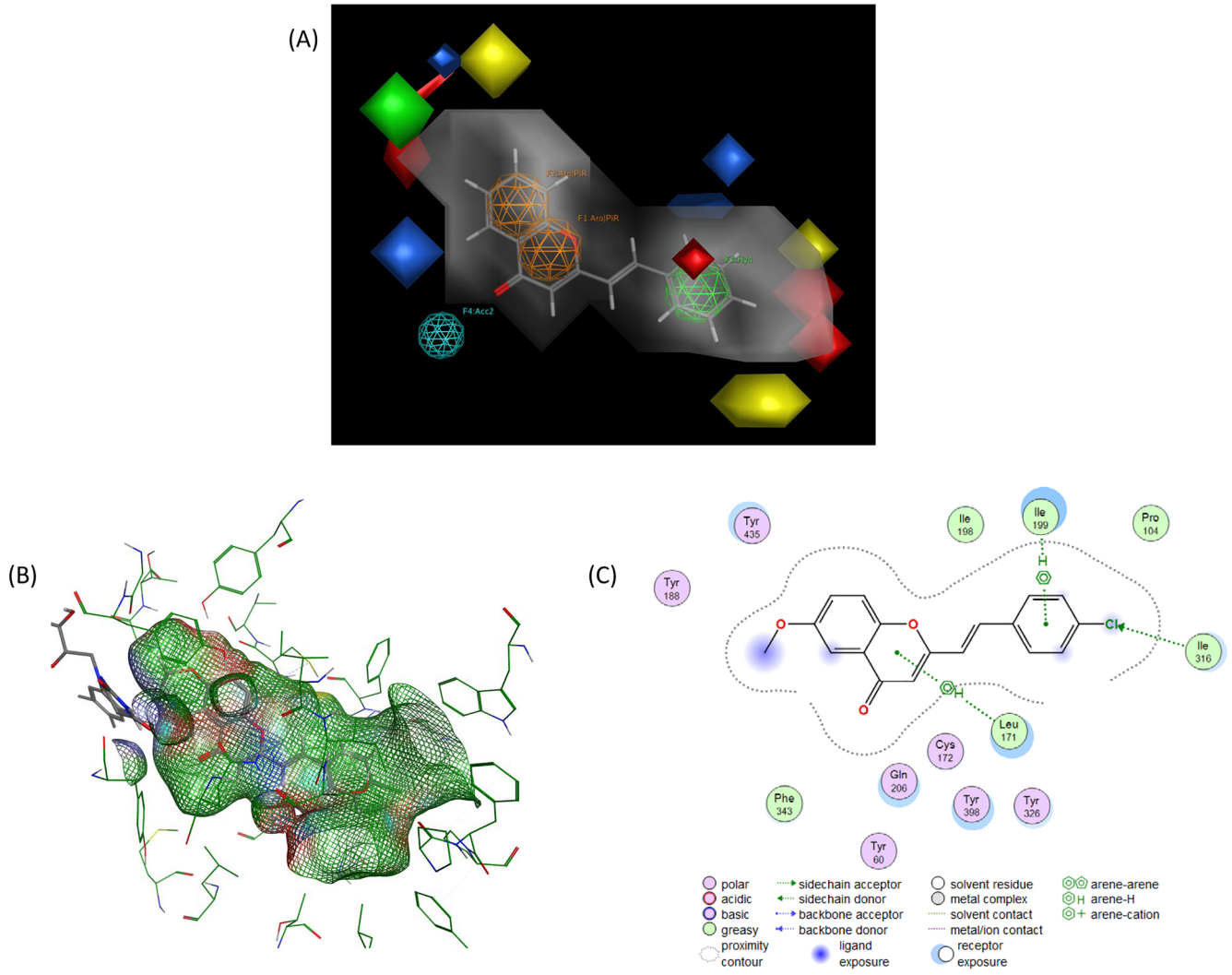

Fig. 7. AutoGPA model and docking results obtained from a set of 2-styrylchromone derivatives as MAO-B inhibitors. (a) AutoGPA steric and electrostatic contours field plot. The position and the structure of 2-styrylchromone is superposed. Green and yellow contours indicate regions where bulky groups increase and decrease activity, respectively. Blue and red contours indicate regions where positive and negative electrostatic groups increase activity. (b) Ligand interaction graph of the active pocket of MAO-B with compound **9**. (c) 2D interaction diagram of compound **9** with the MAO-B binding cavity.

H-5), 7.64 (1H, ddd, J = 8.4, 7.1, 1.7 Hz, H-7), 7.42 (1H, dd, J = 8.4, 1.1 Hz, H-8), 7.38 (1H, ddd, J = 7.9, 7.1, 1.1 Hz, H-6), 6.26 (1H, s, H-3), 2.41 (3H, s, Me). MS (EI) m/z 160 $[M]^+$.

*4.1.3. 2-Methyl-6-methoxy-4H-1-benzopyran-4-one (**IIb**)*

Yield 48%. Pale yellow scaly crystal. mp 107–109 °C (lit. [19] 109–110 °C). ^{1}H NMR ($CDCl_3$, 400 MHz) δ 7.55 (1H, d, J = 3.1 Hz, H-5), 7.36 (1H, d, J = 9.1 Hz, H-8), 7.23 (1H, dd, J = 9.1, 3.1 Hz, H-7), 6.16 (1H, s, H-3), 3.89 (3H, s, OMe), 2.38 (3H, s, Me). MS (EI) m/z 190 $[M]^+$.

*4.1.4. 2-Methyl-7-methoxy-4H-1-benzopyran-4-one (**IIc**)*

Yield 48%. Pale yellow scaly crystal. mp 109–110 °C (lit. [19] 106–108 °C). ^{1}H NMR ($CDCl_3$, 400 MHz) δ 8.08 (1H, d, J = 8.9 Hz, H-5), 6.94 (1H, dd, J = 8.9, 2.4 Hz, H-6), 6.82 (1H, d, J = 2.4 Hz, H-8), 6.11 (1H, s, H-3), 3.90 (3H, s, OMe), 2.36 (3H, s, Me). MS (EI) m/z 190 $[M]^+$.

*4.1.5. Synthesis of (E)-2-styryl-4H-1-benzopyran-4-ones (**1–18**)*

(*E*)-2-Styryl-4*H*-1-benzopyran-4-ones (**1–18**) were synthesized by modifying a previously reported procedure [19]. To a solution of NaOMe (12 mmol) in dry MeOH (12 mL), the corresponding 2-methylchromone (**II**, 2 mmol) and benzaldehyde (**III**, 2.4 mmol) were added. The mixture was refluxed until complete disappearance of the 2-methylchromone (4–8 h). After diluting the reaction mixture with ice-water and acidifying to pH 4 with 2 M HCl, MeOH was removed under reduced pressure. The sample was extracted with CH_2Cl_2. The combined organic layer was dried over Na_2SO_4 and the solvent was evaporated under reduced pressure. The residue was purified by silica gel column chromatography (hexane:AcOEt = 10:1) to give the title compounds.

*4.1.5.1. 2-[(1E)-2-Phenylethenyl]-4H-1-benzopyran-4-one (**1**).* Yield 48%. White needle. mp 142–144 °C. ^{1}H NMR ($CDCl_3$, 400 MHz) δ 8.21 (1H, dd, J = 7.9, 1.7 Hz, H-5), 7.69 (1H, ddd, J = 8.4, 7.1, 1.7 Hz, H-7), 7.63 (1H, d, J = 16.0 Hz, H-β), 7.62–7.59 (2H, m, H-2′, H-6′), 7.55 (1H, dd, J = 8.4, 1.1 Hz, H-8), 7.46–7.37 (4H, m, H-6, H-3′, H-4′, H-5′), 6.81 (1H, d, J = 16.0 Hz, H-α), 6.34 (1H, s, H-3). MS (EI) m/z 248 $[M]^+$. The ^{1}H NMR spectrum was similar to that previously reported [27].

*4.1.5.2. 2-[(1E)-2-(4-Fluorophenyl)ethenyl]-4H-1-benzopyran-4-one (**2**).* Yield 60%. Pale yellow needle. mp 195–198 °C. ^{1}H NMR ($CDCl_3$, 400 MHz) δ 8.20 (1H, dd, J = 7.9, 1.7 Hz, H-5), 7.69 (1H, ddd, J = 8.4,

7.1, 1.7 Hz, H-7), 7.62–7.57 (2H, m, H-2′, H-6′), 7.58 (1H, d, J = 16.0 Hz, H-β), 7.53 (1H, dd, J = 8.5, 1.1 Hz, H-8), 7.40 (1H, ddd, J = 7.9, 7.1, 1.1 Hz, H-6), 7.16–7.10 (2H, m, H-3′, H-5′), 6.72 (1H, d, J = 16.0 Hz, H-α), 6.33 (1H, s, H-3). MS (EI) m/z 266 $[M]^+$. The ^{1}H NMR spectrum was similar to that previously reported [28].

4.1.5.3. 2-[(1E)-2-(4-Chlorophenyl)ethenyl]-4H-1-benzopyran-4-one ***(3)***. Yield 70%. Pale yellow needle. mp 224–226 °C. ^{1}H NMR ($CDCl_3$, 400 MHz) δ 8.20 (1H, dd, J = 7.9, 1.7, H-5), 7.70 (1H, dd, J = 8.4, 7.1 Hz, H-7), 7.57 (1H, d, J = 16.0 Hz, H-β), 7.54 (1H, dd, J = 8.4, 1.1 Hz, H-8), 7.53 (2H, d, J = 8.4 Hz, H-2′, H-6′), 7.41 (1H, ddd, J = 7.9, 7.1, 1.1 Hz, H-6), 7.40 (2H, d, J = 8.4 Hz, H-3′, H-5′), 6.77 (1H, d, J = 16.0 Hz, H-α), 6.34 (1H, s, H-3). MS (EI) m/z 282 $[M]^+$. The ^{1}H NMR spectrum was similar to that previously reported [29].

4.1.5.4. 2-[(1E)-2-(4-Bromophenyl)ethenyl]-4H-1-benzopyran-4-one ***(4)***. Yield 94%. Pale yellow needle. mp 212–216 °C. ^{1}H NMR ($CDCl_3$, 400 MHz) δ 8.20 (1H, dd, J = 7.9, 1.7 Hz, H-5), 7.69 (1H, ddd, J = 8.4, 7.1, 1.7 Hz, H-7), 7.56 (2H, d, J = 8.4 Hz, H-2′, H-6′), 7.55 (1H, d, J = 16.0 Hz, H-β), 7.53 (1H, dd, J = 8.4, 1.1 Hz, H-8), 7.46 (2H, dd, J = 8.4 Hz, H-3′, H-5′), 7.41 (1H, ddd, J = 7.9, 7.1, 1.1 Hz, H-6), 6.79 (1H, d, J = 16.0 Hz, H-α), 6.34 (1H, s, H-3). MS (EI) m/z 326 $[M]^+$. The ^{1}H NMR spectrum was similar to that previously reported [27].

4.1.5.5. 2-[(1E)-2-(4-Methoxyphenyl)ethenyl]-4H-1-benzopyran-4-one ***(5)***. Yield 48%. Yellow needle. mp 139–140 °C. ^{1}H NMR ($CDCl_3$, 400 MHz) δ 8.20 (1H, dd, J = 7.9, 1.7 Hz, H-5), 7.68 (1H, ddd, J = 8.4, 7.1, 1.7 Hz, H-7), 7.58 (1H, d, J = 15.9 Hz, H-β), 7.55 (2H, d, J = 8.7 Hz, H-2′, H-6′), 7.53 (1H, dd, J = 8.4, 1.1 Hz, H-8), 7.39 (1H, ddd, J = 7.9, 7.1, 1.1 Hz, H-6), 6.95 (2H, d, J = 8.7 Hz, H-3′, H-5′), 6.67 (1H, d, J = 15.9 Hz, H-α), 6.31 (1H, s, H-3), 3.87 (3H, s, OMe). MS (EI) m/z 278 $[M]^+$. The ^{1}H NMR spectrum was similar to that previously reported [29].

4.1.5.6. 2-[(1E)-2-(3,4-Dimethoxy)ethenyl]-4H-1-benzopyran-4-one ***(6)***. Yield 58%. Yellow needle. mp 165–166 °C. ^{1}H NMR ($CDCl_3$, 400 MHz) δ 8.20 (1H, dd, J = 7.9, 1.7 Hz, H-5), 7.68 (1H, ddd, J = 8.4, 7.1, 1.7 Hz, H-7), 7.57 (1H, d, J = 16.0 Hz, H-β), 7.53 (1H, dd, J = 8.4, 1.1 Hz, H-8), 7.39 (1H, ddd, J = 7.9, 7.1, 1.1 Hz, H-6), 7.17 (1H, dd, J = 8.3, 2.0 Hz, H-6′), 7.11 (1H, d, J = 2.0 Hz, H-2′), 6.91 (1H, d, J = 8.3 Hz, H-5′), 6.66 (1H, d, J = 16.0 Hz, H-α), 6.32 (1H, s, H-3), 3.98 (3H, s, OMe), 3.94 (3H, s, OMe). MS (EI) m/z 308 $[M]^+$. The ^{1}H NMR spectrum was similar to that previously reported [29].

4.1.5.7. 6-Methoxy-2-[(1E)-2-phenylethenyl]-4H-1-benzopyran-4-one ***(7)***. Yield 71%. Yellow needle. mp 139–140 °C. ^{1}H NMR ($CDCl_3$, 400 MHz) δ 7.61–7.58 (2H, m, H-2′, H-6′), 7.60 (1H, d, J = 16.1 Hz, H-β), 7.58 (1H, d, J = 3.1 Hz, H-5), 7.48 (1H, d, J = 9.1 Hz, H-8), 7.46–7.36 (3H, m, H-3′, H-4′, H-5′), 7.28 (1H, dd, J = 9.1, 3.1 Hz, H-7), 6.80 (1H, d, J = 16.1 Hz, H-α), 6.33 (1H, s, H-3), 3.91 (3H, s, OMe). ^{13}C NMR ($CDCl_3$, 100 MHz) δ 178.3 (C-4), 161.5 (C-2), 156.8 (C-6), 150.8 (C-9), 136.7 (C-β), 135.0 (C-1′), 129.8 (C-4′), 129.0 (C-3′, C-5′), 127.6 (C-2′, C-6′), 124.7 (C-10), 123.7 (C-7), 120.4 (C-α), 119.3 (C-8), 109.9 (C-3), 104.9 (C-5), 56.0 (OMe). MS (EI) m/z 278 $[M]^+$. *Anal.* Calcd for $C_{18}H_{14}O_3$: C, 77.68; H, 5.07. Found: C, 77.91; H, 5.16. MS (EI) m/z 278 $[M]^+$.

4.1.5.8. 2-[(1E)-2-(4-Fluorophenyl)ethenyl]-6-methoxy-4H-1-benzopyran-4-one ***(8)***. Yield 89%. Pale yellow needle. mp 147–150 °C. ^{1}H NMR ($CDCl_3$, 400 MHz) δ 7.60–7.54 (3H, m, H-5, H-2′, H-6′), 7.56 (1H, d, J = 16.0 Hz, H-β), 7.47 (1H, d, J = 9.1 Hz, H-8), 7.28 (1H, dd, J = 9.1, 3.1 Hz, H-7), 7.15–7.09 (2H, m, H-3′, H-5′), 6.71 (1H, d, J = 16.4 Hz, H-α), 6.32 (1H, s, H-3), 3.91 (3H, s, OMe). ^{13}C NMR ($CDCl_3$, 100 MHz) δ 178.3 (C-4), 163.6 (d, $^1J_{C\text{-}F}$ = 250 Hz, C-4′), 161.3 (C-2), 156.9 (C-6), 150.8 (C-9), 135.4 (C-β), 131.3 (d, $^4J_{C\text{-}F}$ = 4 Hz, C-1′), 129.5 (d, $^3J_{C\text{-}F}$ = 8 Hz, C-2′, C-6′), 124.7 (C-10), 123.7 (C-7), 120.1 (C-α), 119.2 (C-8), 116.2 (d, $^2J_{C\text{-}F}$ = 22 Hz, C-3′, C-5′), 109.9 (C-3), 105.0 (C-5), 55.9 (OMe). MS (EI) m/z 296 $[M]^+$. *Anal.* Calcd for $C_{18}H_{13}FO_3$: C, 72.97; H, 4.42. Found: C, 73.16; H, 4.56.

4.1.5.9. 2-[(1E)-2-(4-Chlorophenyl)ethenyl]-6-methoxy-4H-1-benzopyran-4-one ***(9)***. Yield 98%. Pale yellow needle. mp 200–205 °C. ^{1}H NMR ($CDCl_3$, 400 MHz) δ 7.57 (1H, d, J = 3.1 Hz, H-5), 7.55 (1H, d, J = 16.0 Hz, H-β), 7.52 (2H, d, J = 8.5 Hz, H-2′, H-6′), 7.47 (1H, d, J = 9.1 Hz, H-8), 7.41 (2H, d, J = 8.5 Hz, H-3′, H-5′), 7.28 (1H, dd, J = 9.1, 3.1 Hz, H-7), 6.77 (1H, d, J = 16.0 Hz, H-α), 6.33 (1H, s, H-3), 3.90 (3H, s, OMe). ^{13}C NMR ($CDCl_3$, 100 MHz) δ 178.3 (C-4), 161.2 (C-2), 156.9 (C-6), 150.8 (C-9), 135.7 (C-4′), 135.3 (C-β), 133.6 (C-1′), 129.3 (C-3′, C-5′), 128.8 (C-2′, C-6′), 124.7 (C-10), 123.8 (C-7), 120.9 (C-α), 119.3 (C-8), 110.2 (C-3), 105.0 (C-5), 56.0 (OMe). MS (EI) m/z 312 $[M]^+$. *Anal.* Calcd for $C_{18}H_{13}ClO_3$: C, 69.13; H, 4.19. Found: C, 69.03; H, 4.23.

4.1.5.10. 2-[(1E)-2-(4-Bromophenyl)ethenyl]-6-methoxy-4H-1-benzopyran-4-one ***(10)***. Yield 97%. White needle. mp 204–210 °C. ^{1}H NMR ($CDCl_3$, 400 MHz) δ 7.57 (1H, d, J = 3.1 Hz, H-5), 7.56 (2H, d, J = 8.5 Hz, H-2′, H-6′), 7.53 (1H, d, J = 16.0 Hz, H-β), 7.47 (1H, d, J = 9.1 Hz, H-8), 7.45 (2H, d, J = 8.5 Hz, H-3′, H-5′), 7.28 (1H, dd, J = 9.1, 3.1 Hz, H-7), 6.78 (1H, d, J = 16.1 Hz, H-α), 6.33 (1H, s, H-3), 3.91 (3H, s, OMe). ^{13}C NMR ($CDCl_3$, 100 MHz) δ 178.3 (C-4), 161.1 (C-2), 156.9 (C-6), 150.8 (C-9), 135.3 (C-β), 134.0 (C-1′), 132.2 (C-3′, C-5′), 129.0 (C-2′, C-6′), 124.7 (C-10), 123.9 (C-4′), 123.8 (C-7), 121.0 (C-α), 119.3 (C-8), 110.2 (C-3), 105.0 (C-5), 56.0 (OMe). MS (EI) m/z 356 $[M]^+$. *Anal.* Calcd for $C_{18}H_{13}BrO_3$: C, 60.52; H, 3.67. Found: C, 60.32; H, 3.68.

4.1.5.11. 6-Methoxy-2-[(1E)-2-(4-methoxyphenyl)ethenyl]-4H-1-benzopyran-4-one ***(11)***. Yield 73%. Yellow needle. mp 138–140 °C. ^{1}H NMR ($CDCl_3$, 400 MHz) δ 7.57 (1H, d, J = 3.1 Hz, H-5), 7.55 (1H, d, J = 16.0 Hz, H-β), 7.54 (2H, d, J = 8.6 Hz, H-2′, H-6′), 7.46 (1H, d, J = 9.1 Hz, H-8), 7.26 (1H, dd, J = 9.1, 3.1 Hz, H-7), 6.94 (2H, d, J = 8.6 Hz, H-3′, H-5′), 6.66 (1H, d, J = 16.0 Hz, H-α), 6.29 (1H, s, H-3), 3.90 (3H, s, OMe), 3.86 (3H, s, OMe). MS (EI) m/z 308 $[M]^+$. The ^{1}H NMR spectrum was similar to that previously reported [30].

4.1.5.12. 2-[(1E)-2-(3,4-Dimethoxy)ethenyl]-6-methoxy-4H-1-benzopyran-4-one ***(12)***. Yield 78%. Yellow needle. mp 159–161 °C. ^{1}H NMR ($CDCl_3$, 400 MHz) δ 7.58 (1H, d, J = 3.1 Hz, H-5), 7.54 (1H, d, J = 16.0 Hz, H-β), 7.46 (1H, d, J = 9.1 Hz, H-8), 7.27 (1H, dd, J = 9.1, 3.1 Hz, H-7), 7.17 (1H, dd, J = 8.3, 2.0 Hz, H-6′), 7.11 (1H, d, J = 2.0 Hz, H-2′), 6.91 (1H, d, J = 8.3 Hz, H-5′), 6.65 (1H, d, J = 16.0 Hz, H-α), 6.31 (1H, s, H-3) , 3.97 (3H, s, OMe), 3.94 (3H, s, OMe), 3.91 (3H, s, OMe), ^{13}C NMR ($CDCl_3$, 100 MHz) δ 178.3 (C-4), 161.9 (C-2), 156.8 (C-6), 150.8 (C-9, C-4′), 149.3 (C-3′), 136.7 (C-β), 128.1 (C-1′), 124.7 (C-10), 123.6 (C-7), 122.0 (C-6′), 119.2 (C-8), 118.1 (C-α), 111.2 (C-5′), 109.3 (C-3, C-2′), 105.0 (C-5), 56.01 (OMe), 55.99 (OMe), 55.95 (OMe). MS (EI) m/z 338 $[M]^+$. *Anal.* Calcd for $C_{20}H_{18}O_5$: C, 71.00; H, 5.36. Found: C, 71.09; H, 5.24.

4.1.5.13. 7-Methoxy-2-[(1E)-2-phenylethenyl]-4H-1-benzopyran-4-one ***(13)***. Yield 77%. Yellow prism. mp 192–194 °C. ^{1}H NMR ($CDCl_3$, 400 MHz) δ 8.10 (1H, d, J = 8.5 Hz, H-5), 7.61–7.57 (2H, m, H-2′, H-6′), 7.58 (1H, d, J = 16.1 Hz, H-β), 7.46–7.36 (3H, m, H-3′, H-4′, H-5′), 6.98–6.94 (2H, m, H-6, H-8), 6.77 (1H, d, J = 16.1 Hz, H-α), 6.27 (1H, s, H-3), 3.94 (3H, s, OMe); MS (EI) m/z 278 $[M]^+$. The ^{1}H NMR spectrum was similar to that previously reported [31].

4.1.5.14. 2-[(1E)-2-(4-Fluorophenyl)ethenyl]-7-methoxy-4H-1-benzopyran-4-one ***(14)***. Yield 66%. Pale light brown needle. mp 170–175 °C. ^{1}H NMR ($CDCl_3$, 400 MHz) δ 8.10 (1H, d, J = 8.8 Hz, H-5), 7.59–7.54 (2H, m, H-2′, H-6′), 7.54 (1H, d, J = 15.9 Hz, H-β), 7.15–7.19 (2H, m, H-3′, H-5′), 6.97 (1H, dd, J = 8.8, 2.4 Hz, H-6), 6.94

(1H, d, J = 2.4 Hz, H-8), 6.69 (1H, d, J = 15.9 Hz, H-α), 6.26 (1H, s, H-3), 3.94 (3H, s, OMe). ^{13}C NMR ($CDCl_3$, 100 MHz) δ 177.8 (C-4), 164.2 (C-7), 163.5 (d, $^1J_{C\text{-}F}$ = 250 Hz, C-4′), 161.2 (C-2), 157.7 (C-9), 135.0 (C-β), 131.4 (d, $^4J_{C\text{-}F}$ = 4 Hz, C-1′), 129.4 (d, $^3J_{C\text{-}F}$ = 8 Hz, C-2′, C-6′), 127.1 (C-5), 120.1 (C-α), 118.0 (C-10), 116.1 (d, $^2J_{C\text{-}F}$ = 22 Hz, C-3′, C-5′), 114.1 (C-6), 110.7 (C-3), 100.3 (C-8), 55.8 (OMe). MS (EI) m/z 296 $[M]^+$. *Anal.* Calcd for $C_{18}H_{13}FO_3$: C, 72.97; H, 4.42. Found: C, 73.11; H, 4.52.

4.1.5.15. 2-[(1E)-2-(4-Chlorophenyl)ethenyl]-7-methoxy-4H-1-benzopyran-4-one ***(15)***. Yield 95%. Pale light brown needle. mp 199–203 °C. ^{1}H NMR ($CDCl_3$, 400 MHz) δ 8.10 (1H, d, J = 8.8 Hz, H-5), 7.52 (1H, d, J = 16.0 Hz, H-β), 7.51 (2H, d, J = 8.6 Hz, H-2′, H-6′), 7.39 (2H, d, J = 8.6 Hz, H-3′, H-5′), 6.97 (1H, dd, J = 8.8, 2.4 Hz, H-6), 6.93 (1H, d, J = 2.4 Hz, H-8), 6.74 (1H, d, J = 16.0 Hz, H-α), 6.27 (1H, s, H-3), 3.94 (3H, s, OMe). ^{13}C NMR ($CDCl_3$, 100 MHz) δ 177.8 (C-4), 164.2 (C-7), 161.0 (C-2), 157.7 (C-9), 135.6 (C-4′), 134.9 (C-β), 133.6 (C-1′), 129.3 (C-3′, C-5′), 128.7 (C-2′, C-6′), 127.1 (C-5), 120.9 (C-α), 118.0 (C-10), 114.1 (C-6), 111.0 (C-3), 100.3 (C-8), 55.9 (OMe). MS (EI) m/z 312 $[M]^+$. *Anal.* Calcd for $C_{18}H_{13}ClO_3$: C, 69.13; H, 4.19. Found: C, 69.00; H, 4.15.

4.1.5.16. 2-[(1E)-2-(4-Bromophenyl)ethenyl]-7-methoxy-4H-1-benzopyran-4-one ***(16)***. Yield 98%. White needle. mp 204–210 °C. ^{1}H NMR ($CDCl_3$, 400 MHz) δ 8.10 (1H, d, J = 8.8 Hz, H-5), 7.56 (2H, d, J = 8.5 Hz, H-2′, H-6′), 7.51 (1H, d, J = 16.0 Hz, H-β), 7.44 (2H, d, J = 8.5 Hz, H-3′, H-5′), 6.97 (1H, dd, J = 8.8, 2.4 Hz, H-6), 6.93 (1H, d, J = 2.4 Hz, H-8), 6.94 (1H, d, J = 2.4 Hz, H-8), 6.76 (1H, d, J = 16.0 Hz, H-α), 6.27 (1H, s, H-3), 3.94 (3H, s, OMe). ^{13}C NMR ($CDCl_3$, 100 MHz) δ 177.8 (C-4), 164.2 (C-7), 160.9 (C-2), 157.7 (C-9), 134.9 (C-β), 134.0 (C-1′), 132.2 (C-3′, C-5′), 129.0 (C-2′, C-6′), 127.1 (C-5), 123.9 (C-4′), 121.0 (C-α), 118.0 (C-10), 114.1 (C-6), 111.0 (C-3), 100.3 (C-8), 55.8 (OMe). MS (EI) m/z 356 $[M]^+$. *Anal.* Calcd for $C_{18}H_{13}BrO_3$: C, 60.52; H, 3.67. Found: C, 60.77; H, 3.65.

4.1.5.17. 7-Methoxy-2-[(1E)-2-(4-methoxyphenyl)ethenyl]-4H-1-benzopyran-4-one ***(17)***. Yield 67%. Brown needle. mp 128–129 °C. ^{1}H NMR ($CDCl_3$, 400 MHz) δ 8.10 (1H, d, J = 8.6 Hz, H-5), 7.54 (1H, d, J = 16.0 Hz, H-β), 7.53 (2H, d, J = 8.9 Hz, H-2′, H-6′), 6.98–6.93 (2H, m, H-6, H-8), 6.95 (2H, d, J = 8.9 Hz, H-3′, H-5′), 6.64 (1H, d, J = 16.0 Hz, H-α), 6.23 (1H, s, H-3), 3.93 (3H, s, OMe), 3.86 (3H, s, OMe). ^{13}C NMR ($CDCl_3$, 100 MHz) δ 177.9 (C-4), 164.1 (C-7), 161.8 (C-4′), 161.0 (C-2), 157.7 (C-9), 136.0 (C-β), 129.2 (C-2′, C-6′), 127.9 (C-1′), 127.0 (C-5), 118.04 (C-10), 117.96 (C-α), 114.5 (C-3′, C-5′), 113.9 (C-6), 109.9 (C-3), 100.3 (C-8), 55.8 (OMe), 55.4 (OMe). MS (EI) m/z 308 $[M]^+$. *Anal.* Calcd for $C_{19}H_{16}O_4$: C, 74.01; H, 5.23. Found: C, 74.16; H, 5.21.

4.1.5.18. 2-[(1E)-2-(3,4-Dimethoxy)ethenyl]-7-methoxy-4H-1-benzopyran-4-one ***(18)***. Yield 67%. Yellow needle. mp 198–199 °C. ^{1}H NMR ($CDCl_3$, 400 MHz) δ 8.10 (1H, d, J = 8.7 Hz, H-5), 7.52 (1H, d, J = 16.0 Hz, H-β), 7.17 (1H, dd, J = 8.3, 2.0 Hz, H-6′), 7.10 (1H, d, J = 2.0 Hz, H-2′), 6.96 (1H, dd, J = 8.7, 2.3 Hz, H-6), 6.93 (1H, d, J = 2.3 Hz, H-8), 6.91 (1H, d, J = 8.3 Hz, H-5′), 6.63 (1H, d, J = 16.0 Hz, H-α), 6.25 (1H, s, H-3), 3.97 (3H, s, OMe), 3.93 (6H, s, OMe). ^{13}C NMR ($CDCl_3$, 100 MHz) δ 177.9 (C-4), 164.1 (C-7), 161.7 (C-2), 157.7 (C-9), 150.7 (C-4′), 149.3 (C-3′), 136.3 (C-β), 128.1 (C-1′), 127.1 (C-5), 122.0 (C-6′), 118.1 (C-α), 118.0 (C-10), 113.9 (C-6), 111.2 (C-5′), 110.0 (C-3), 109.3 (C-2′), 100.3 (C-8), 56.01 (OMe), 55.99 (OMe), 55.8 (OMe). MS (EI) m/z 338 $[M]^+$. *Anal.* Calcd for $C_{20}H_{18}O_5$: C, 71.00; H, 5.36. Found: C, 71.09; H, 5.32.

4.2. Biological assays

Recombinant human monoamine oxidase A (MAO-A), recombinant human MAO-B, pargyline and kynuramine were purchased from Sigma-Aldrich Japan Co., Tokyo, Japan.

4.3. MAO inhibitory assay

MAO inhibitory activity was assayed using the method of Novaroli *et al.* [32] with minor modifications. Briefly, 140 µL of 0.1 M potassium phosphate buffer (pH 7.4), 8 µL of 0.75 mM kynuramine, and 2 µL of a dimethyl sulfoxide (DMSO) inhibitor solution, were preincubated at 37 °C for 10 min. Diluted human recombinant enzyme (50 µL) was then added to obtain a final protein concentration of 0.0075 mg/mL (MAO-A) or 0.015 mg/mL (MAO-B) in the assay mixture. The reaction mixture was further incubated at 37 °C and the reaction was stopped after 20 min by the addition of 75 µL of 2 M NaOH. The product generated by MAO, 4-quinolinol, is fluorescent and was measured at *Ex* 310 nm/*Em* 400 nm using a microplate reader (Molecular Devices SPECTRA MAX M2). Each data point was measured from triplicate samples. The sample solution was replaced with DMSO to provide a negative control and pargyline was used as a positive control. The IC_{50} values were calculated from a line through two points that sandwiched the point corresponding to 50% inhibition (IC_{50}) by plotting the remained activity (%) related to the control (100%) versus the logarithm of the inhibitor concentration to obtain a sigmoidal dose-response curve.

4.4. Lineweaver–Burk plots

This analysis was conducted according to the method reported by Meiring *et al.* [20]. The inhibition of MAO-B by compound **9** was determined by constructing a set of four Lineweaver–Burk plots. The first plot was constructed in the absence of inhibitor and the remaining three plots were constructed in the presence of various concentrations of the test inhibitor: $1/4 \times IC_{50}$, $1/2 \times IC_{50}$, $1 \times IC_{50}$ and $2 \times IC_{50}$ (IC_{50} = 0.017 µM). The enzyme substrate kynuramine was used at concentrations ranging from 3.75 to 120 µM.

4.5. Analysis of the reversibility of MAO-B inhibition (dilution method).

This analysis was conducted according to the method reported by Meiring *et al.* [20]. Briefly, compound **9** (IC_{50} = 0.017 µM) at concentrations equal to $10 \times IC_{50}$ and $100 \times IC_{50}$ was preincubated with MAO-B (0.15 mg/mL) for 30 min at 37 °C. These preincubations contained DMSO (4%) as co-solvent. The reaction mixtures were subsequently diluted 10-fold by adding a solution of kynuramine to yield final concentrations of the test inhibitor equal to $1 \times IC_{50}$ and $0.1 \times IC_{50}$. After dilution, the final concentration of kynuramine was 30 µM and the final concentration of MAO-B was 0.015 mg/mL. The reaction mixtures were incubated for a further 20 min at 37 °C, the reactions were terminated, and the formation of 4-hydroxyquinoline was measured as described above. For comparison, pargyline (IC_{50} = 0.22 µM) at a concentration of $10 \times IC_{50}$ was similarly preincubated with MAO-B, diluted to $1 \times IC_{50}$, and residual MAO-B activity was measured as above. Similar reactions served as controls and were conducted in the absence of inhibitor.

4.6. Calculation of chemical descriptors

Each 3D chemical structure (Marvin Sketch ver 16; ChemAxon, Budapest, Hungary, http://www.chemaxon.com) was optimized by CORINA Classic (Molecular Networks GmbH, Nürnberg, Germany) with forcefield calculations (amber-10: EHT) in Molecular Operating Environment (MOE) version 2018.0101 (Chemical Computing Group Inc., Quebec, Canada). The number of structural descriptors calculated from MOE [21] and Dragon 7.0 [22] (Kode srl., Pisa, Italy) was 344 and 5255, respectively, of which 279 and 2827 (total 3106) descriptors were used for analysis.

4.7. 3D-QSAR and docking analyses

AutoGPA in MOE can automatically generate 3D-QSAR models

based on the chemical structures and biological activities for sets of inhibitors [24,25]. The CoMFA analysis algorithm was employed to develop 3D-QSAR models [23]. Docking analysis was carried out with MAO-B protein (PDB code 4A79) using MOE.

4.8. Statistical analysis

The relation between the substituents and the MAO related properties such as IC_{50} values and MAO-B selectivity was analyzed with Wilcoxon signed-rank test. The relation between the chemical descriptors and the MAO-B related properties was investigated using Pearson's correlation analysis. These statistical calculations were performed by JMP Pro version 14.0.0 (SAS Institute Inc., Cary, NC, USA). The significance level was set at $p < 0.05$.

Appendix A. Supplementary material

Supplementary data to this article can be found online at https://doi.org/10.1016/j.bioorg.2019.103285.

References

[1] A.S. Kalgutkar, N. Castagnoli Jr., Selective inhibitors of monoamine oxidase (MAO-A and MAO-B) as probes of its catalytic site and mechanism, Med. Res. Rev. 15 (4) (1995) 325–388.

[2] D.E. Edmondson, L. DeColibus, C. Binda, M. Li, A. Mattevi, New insights into the structures and functions of human monoamine oxidases A and B, J. Neural Transm. 114 (6) (2007) 703–705, https://doi.org/10.1007/s00702-007-0674-z.

[3] L. De Colibus, M. Li, C. Binda, A. Lustig, D.E. Edmondson, A. Mattevi, Three-dimensional structure of human monoamine oxidase A (MAO A): relation to the structures of rat MAO A and human MAO B, Proc. Natl. Acad. Sci. U. S. A. 102 (36) (2005) 12684–12689 g 29.

[4] S. Schedin-Weiss, M. Inoue, L. Hromadkova, Y. Teranishi, N.G. Yamamoto, B. Wiehager, N. Bogdanovic, B. Winblad, A. Sandebring-Matton, S. Frykman, L.O. Tjernberg, Monoamine oxidase B is elevated in Alzheimer disease neurons, is associated with γ-secretase and regulates neuronal amyloid β-peptide levels, Alzheimers Res. Ther. 9 (1) (2017) 57, https://doi.org/10.1186/s13195-017-0279-1.

[5] A. Gaspar, M.J. Matos, J. Garrido, E. Uriarte, F. Borges, Chromone: a valid scaffold in medicinal chemistry, Chem. Rev. (114(9), 2014,) 4960–4992, https://doi.org/10.1021/cr400265z.

[6] J. Reis, A. Gaspar, N. Milhazes, F. Borges, Chromone as a privileged scaffold in drug discovery, Recent Adv., J. Med. Chem. 60 (19) (2017) 7941–7957, https://doi.org/10.1021/acs.jmedchem.6b01720.

[7] A. Gaspar, T. Silva, M. Yáñez, D. Vina, F. Orallo, F. Ortuso, E. Uriarte, S. Alcaro, F. Borges, Chromone a privileged scaffold for the development of monoamine oxidase inhibitors, J. Med. Chem. 54 (14) (2011) 5165–5173, https://doi.org/10.1021/jm2004267.

[8] C.M.M. Santos, A.M.S. Silva, An overview of 2-styrylchromones: natural occurrence, synthesis, reactivity and biological properties, Eur. J. Org. Chem. 2017 (22) (2017) 3115–3133.

[9] A. Gomes, M. Freitas, E. Fernandes, J.L. Lima, Biological activities of 2-styrylchromones, Mini Rev. Med. Chem. 10 (1) (2010) 1–7.

[10] M. Koushki, N. Amiri-Dashatan, N. Ahmadi, H.A. Abbaszadeh, M. Rezaei-Tavirani, Resveratrol: A miraculous natural compound for diseases treatment, Food Sci. Nutr. 6 (8) (2018) 2473–2490, https://doi.org/10.1002/fsn3.855 eCollection 2018 Nov.

[11] B. Salehi, A.P. Mishra, M. Nigam, B. Sener, M. Kilic, M. Sharifi-Rad, P.V.T. Fokou, N. Martins, J. Sharifi-Rad, Resveratrol: a double-edged sword in health benefits, pii: E91, Biomedicines 6 (3) (2018), https://doi.org/10.3390/biomedicines6030091.

[12] M. Yáñez, N. Fraiz, E. Cano, F. Orallo, Inhibitory effects of cis- and trans-resveratrol on noradrenaline and 5-hydroxytryptamine uptake and on monoamine oxidase activity, Biochem. Biophys. Res. Commun. 344 (2) (2006) 688–695.

[13] A. Ozaita, G. Olmos, M.A. Boronat, J.M. Lizcano, M. Unzeta, J.A. García-Sevilla, Inhibition of monoamine oxidase A and B activities by imidazol(ine)/guanidine drugs, nature of the interaction and distinction from I2-imidazoline receptors in rat liver, Br. J. Pharmacol. 121 (5) (1997) 901–912.

[14] J.F. Chen, S. Steyn, R. Staal, J.P. Petzer, K. Xu, C.J. Van Der Schyf, K. Castagnoli, P.K. Sonsalla, N. Castagnoli Jr, M.A. Schwarzschild, 8-(3-Chlorostyryl)caffeine may attenuate MPTP neurotoxicity through dual actions of monoamine oxidase inhibition and A2A receptor antagonism, J. Biol. Chem. 277 (39) (2002) 36040–36044.

[15] D. Van den Berg, K.R. Zoellner, M.O. Ogunrombi, S.F. Malan, G. Terre'Blanche, N. Castagnoli Jr, J.J. Bergh, J.P. Petzer, Inhibition of monoamine oxidase B by selected benzimidazole and caffeine analogues, Bioorg. Med. Chem. 15 (11) (2007) 3692–3702.

[16] E.M. Van der Walt, E.M. Milczek, S.F. Malan, D.E. Edmondson, N. Castagnoli Jr, J.J. Bergh, J.P. Petzer, Inhibition of monoamine oxidase by (E)-styrylisatin analogues, Bioorg. Med. Chem. Lett. 19 (9) (2009,) 2509–2513, https://doi.org/10.1016/j.bmcl.2009.03.030.

[17] M.M. Van der Walt, G. Terre'Blanche, A. Petzer, A.C. Lourens, J.P. Petzer, The adenosine A(2A) antagonistic properties of selected C8-substituted xanthines, Bioorg. Chem. 49 (2013) 49–58, https://doi.org/10.1016/j.bioorg.2013.06.006.

[18] K. Takao, H. Yahagi, Y. Uesawa, Y. Sugita, 3-(E)-Styryl-2H-chromene derivatives as potent and selective monoamine oxidase B inhibitors, Bioorg. Chem. 77 (2018) 436–442, https://doi.org/10.1016/j.bioorg.2018.01.036.

[19] A.Y. Shaw, C.Y. Chang, H.H. Liau, P.J. Lu, H.L. Chen, C.N. Yang, H.Y. Li, Synthesis of 2-styrylchromones as a novel class of antiproliferative agents targeting carcinoma cells, Eur. J. Med. Chem. 44 (6) (2009) 2552–2562, https://doi.org/10.1016/j.ejmech.2009.01.034.

[20] L. Meiring, J.P. Petzer, A. Petzer, Inhibition of monoamine oxidase by 3,4-dihydro-2(1H)-quinolinone derivatives, Bioorg. Med. Chem. Lett. 23 (20) (2013) 5498–5502, https://doi.org/10.1016/j.bmcl.2013.08.071.

[21] Calculate Descriptors, MOE2015.10 on-line help manual, Chemical Computing Group.

[22] https://chm.kode-solutions.net/products_dragon_descriptors.php.

[23] R.D. Cramer, D.E. Patterson, J.D. Bunce, Comparative molecular field analysis (CoMFA). 1. Effect of shape on binding of steroids to carrier proteins, J. Am. Chem. Soc. 110 (18) (1988) 5959–5967, https://doi.org/10.1021/ja00226a005.

[24] N. Asakawa, S. Kobayashi, J. Goto, N. Hirayama, AutoGPA: an automated 3D-QSAR method based on pharmacophore alignment and grid potential analysis, Int. J. Med. Chem. 2012 (2012), https://doi.org/10.1155/2012/498931.

[25] F.Y. Guo, Q.Y. Yan, K. Lin, W.Y. Hong, G.S. Yang, AutoGPA-based 3D-QSAR modeling and molecular docking study on factor Xa inhibitors as anticoagulant agents, MATEC Web Conf. 44 (2016) 02018.

[26] L.G. Iacovino, F. Magnani, C. Binda, The structure of monoamine oxidases: past, present, and future, J. Neural. Transm. (Vienna) 125 (11) (2018) 1567–1579, https://doi.org/10.1007/s00702-018-1915-z.

[27] W. Huang, Y. Ding, Y. Miao, M.Z. Liu, Y. Li, G.F. Yang, Synthesis and antitumor activity of novel dithiocarbamate substituted chromones, Eur. J. Med. Chem. 44 (9) (2009,) 3687–12696, https://doi.org/10.1016/j.ejmech.2009.04.004.

[28] M. Momin, D. Ramjugernath, N.A. Koorbanally, Structure elucidation of a series of fluoro-2-styrylchromones and methoxy-2-styrylchromones using 1D and 2D NMR spectroscopy, Magn. Reson. Chem. 52 (2014) 521–529.

[29] C. Lin, P.-J. Lu, C.-N. Yang, C. Hulme, A.Y. Shaw, Structure-activity relationship study of growth inhibitory 2-styrylchromones against carcinoma cells, Med. Chem. Res. 22 (5) (2013) 2385–2394.

[30] Rao V. Madhava, B. Ujwala, P. Priyadarshini, Murthy P. Krishna, Synthesis, antioxidant and antimicrobial activity of three new 2-styrylchromones and their analogues, Der Pharma Chemica 8 (7) (2016) 1–6 ISSN 0975-413X.

[31] S.R. Goel, J.K. Makrandi, Microwave assisted synthesis of 1-(2-hydroxyphenyl)-5-phenyl pent-4-ene-1,3-diones and their conversion to 2-styryl chromones, Ind. J. Chem. 45B (5) (2006) 1278–1281.

[32] L. Novaroli, M. Reist, E. Favre, A. Carotti, M. Catto, P.A. Carrupt, Human recombinant monoamine oxidase B as reliable and efficient enzyme source for inhibitor screening, Bioorg. Med. Chem. 13 (22) (2005) 6212–6217.